



LUND UNIVERSITY

On the automation of thermographic phosphor calibration

About Nada, Fahd Jouda; Knappe, Christoph; Xu, Xin; Richter, Mattias; Aldén, Marcus

Published in:
Proceedings of the 60th International Instrumentation Symposium

2014

[Link to publication](#)

Citation for published version (APA):

About Nada, F. J., Knappe, C., Xu, X., Richter, M., & Aldén, M. (in press). On the automation of thermographic phosphor calibration. In *Proceedings of the 60th International Instrumentation Symposium* Institution of Engineering and Technology.

Total number of authors:
5

General rights

Unless other specific re-use rights are stated the following general rights apply:
Copyright and moral rights for the publications made accessible in the public portal are retained by the authors and/or other copyright owners and it is a condition of accessing publications that users recognise and abide by the legal requirements associated with these rights.

- Users may download and print one copy of any publication from the public portal for the purpose of private study or research.
- You may not further distribute the material or use it for any profit-making activity or commercial gain
- You may freely distribute the URL identifying the publication in the public portal

Read more about Creative commons licenses: <https://creativecommons.org/licenses/>

Take down policy

If you believe that this document breaches copyright please contact us providing details, and we will remove access to the work immediately and investigate your claim.

LUND UNIVERSITY

PO Box 117
221 00 Lund
+46 46-222 00 00

On the automation of thermographic phosphor calibration

F. Abou Nada, C. Knappe, X. Xu, M. Richter and M. Aldén

Department of Physics, Division of Combustion Physics, Lund University, Box 118, S-22100, Lund, Sweden

E-mail: Fahed.Abou_Nada@forbrf.lth.se

Keywords: thermographic phosphors, calibration, thermometry.

Abstract

Thermographic phosphors can be robust temperature remote sensors. The accuracy of the temperature measured by the phosphor is highly dependent on the quality of the phosphor calibration used. Conventionally, thermographic phosphors are calibrated by measuring a series of decay curves at known stable oven temperatures. The process is then repeated covering the thermal sensitivity range of the phosphor chosen. Heating and cooling rates of high temperature ovens are usually low. Also, thermal equilibrium of the system is required at each calibration temperature before acquiring luminescence decay curves. Thus, the process is usually time consuming and the number of calibration points achieved is limited to a couple of dozen points. This study presents and validates the development of an automatic routine for the calibration of thermographic phosphors. It was designed to continuously and simultaneously acquire phosphor decay curves along with their corresponding thermocouple temperatures. The developed routine required software and hardware improvements. An updated design of the calibration substrate was implemented to improve the thermal conditions during calibration. Thermal gradients were further studied using a heat transfer model. The routine implemented a specially designed sparsing algorithm that reduced the sampling rate of the decaying luminescence curve without influencing the calculated decay time. The upper heating rate is set at $4 \text{ K} \cdot \text{min}^{-1}$ due to limitation imposed by the ceramic calibration oven. The phosphors CdWO_4 and $\text{Mg}_3\text{F}_2\text{GeO}_4\text{:Mn}$ were chosen to validate the finalized routine. After the completion of the calibration process, a library-based calibration is created as the final product. The automated calibration routine delivered an overall accuracy improvement of 1-2 K, reduced calibration duration by factor of four and provided the possibility of deriving signal recognition algorithms. The condensed calibration dataset produced by the proposed calibration routine was further employed to develop a novel signal shape recognition algorithm for temperature evaluation.

1 Introduction

Temperature is a highly important parameter in numerous processes. Measuring temperature with high precision and accuracy is a task involving a great deal of challenges.

Obtaining sub-kelvin accuracy, demands a great deal of effort and precautions from possible sources of error. Childs et al provided a concise summary of current available temperature measurement techniques accompanied by a comprehensive comparison [1]. The selection of a suitable technique depends on the requirements. Factors such as accuracy, resolution, temperature range, cost, stability, and tolerance to the conditions of the probed environment, suggest the most adequate technique for the addressed experiment. Also, attention to possible sources of error is necessary. Errors can originate from temperature gradients across the material whose temperature is measured, poor thermal contact, self-heating, radiant energy loss, and calibration drifts. The majority of temperature sensors except, infra-red radiation based sensors require full contact with the medium being measured, thus complicating their applicability to reciprocating and rotating objects.

During the last decades, a new temperature sensing technique, known as phosphor thermometry (PT), has been developed and applied in a variety of applications. Phosphor thermometry utilizes temperature sensitive powders that are usually mixed with a high-temperature binder and then applied to the object of interest. PT can offer advantages over other sensing methods, because of its limited intrusiveness, remote probing capability, practicality, and survivability in harsh environmental conditions. Most thermographic phosphors (TP) consist of a host material that is doped with an activator material. The activator material most often belongs to rare-earth ions or transition metals groups [2].

Thermographic phosphors exhibit a change of the optical emission characteristics with temperature. The nature of the characteristic change observed can be spectral, temporal, or both. Spectral changes manifest as a change in the intensity of in the emission spectrum. Using the ratio of two spectral bands, a relation between the measured ratio and temperature is constructed. This relation is later used to calculate the temperature of the TP. On the other hand, a temporal change is usually seen as the decrease in the decay time of the luminescent emission after excitation by a pulsed radiation source. The luminescence decay time is mapped against temperature, resulting in a similar relation to that established for the spectral ratio method.

Two-dimensional detectors, such as charge-coupled detectors (CCDs) and complementary metal-oxide-semiconductor (CMOS) detectors are used to capture TP emission changes and obtain 2-D temperature maps. While detectors such as photomultiplier tubes (PMTs), micro-channel plate PMT

(MCP-PMT), and avalanche photodiodes are used to obtain point temperature measurements.

Phosphor calibration is considered the backbone of the PT technique and a potential source of bias error. The quality of the calibration directly affects the accuracy of the measured temperatures. Similar to other temperature sensors, highly accurate calibration procedures are necessary to make PT a dependable temperature sensing technique.

Conventionally, thermographic phosphors calibrations are achieved by coating a thin layer of phosphor on top of a metallic substrate whose temperature is monitored using thermocouples. The phosphor-coated substrate is heated using an electric oven and the calibration process is commenced as the following. First, the oven is heated to a preassigned temperature. A waiting period is necessary for the system to reach thermal equilibrium to ensure that no thermal gradients are present. When thermal equilibrium is reached, a series of measurements are acquired, usually around 100 single acquisitions, and then averaged to create a single data point. The same procedure is repeated at each of the chosen calibration temperatures until the desired temperature calibration range is covered. This process is time consuming due to the system thermal equilibrium requirement. Also, for practical reasons, it suffers from low density of data points in the calibration curve necessitating the usage of interpolating functions to provide a complete calibration function.

The automated calibration, described in this work, was designed to continuously acquire the decay curves of the phosphorescence while logging the temperatures measured by the thermocouples plugged into the substrate. The new calibration system involved the development of a new substrate design and a novel automatic routine. The heat transfer is modelled, using a finite element method, to analyse the thermal gradients within the substrate. Two TPs, CdWO_4 and $\text{Mg}_3\text{F}_2\text{GeO}_4\text{:Mn}$, were employed to test the developed system. The objective of this study is to establish a system capable of delivering a high-quality library-based calibration leading to improvements in calibration accuracy and reduction in calibration duration. Furthermore, the high data density provided by the achieved calibration creates the possibility of using signal shape recognition algorithms as a practical alternative to conventional decay-curve-fitting algorithms.

2 Experimental procedures

2.1 Experimental setup

The description of the setup is divided into a hardware and a software section. The properties of the thermographic phosphor employed are also defined, along with the conditions and parameters used in the heat transfer equation solver.

2.1.1 Hardware

The hardware components of the calibration system are the following; pulsed UV laser, oven, substrate, thermocouples, data acquisition unit (DAQ), oscilloscope, and PMT. CdWO_4

and $\text{Mg}_3\text{F}_2\text{GeO}_4\text{:Mn}$ were excited using temporally short UV pulses at 266 nm and 355 nm respectively. The temporal width of the pulses is 6 ns. The laser is operated at 10 Hz repetition rate. CdWO_4 has a broad emission spectrum centred at 460 nm, while $\text{Mg}_3\text{F}_2\text{GeO}_4\text{:Mn}$ has an emission spectrum with a strong spectral band in the red region with several distinctive peaks (Fig.1).

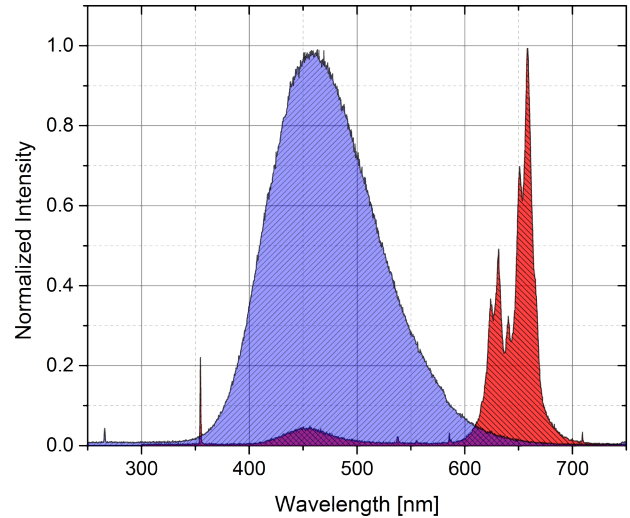


Figure 1. Emission spectra of CdWO_4 (blue) and $\text{Mg}_3\text{F}_2\text{GeO}_4\text{:Mn}$ (red) thermographic phosphors after excitation by UV laser radiation at 266 nm and 355 nm respectively.

The substrate was built from high-performance alloy (Hastelloy C-4). The substrate was designed in a shape of a disk that has a diameter of 41 mm and thickness of 6 mm. Several factors were taken into consideration when designing the substrate, factors such as errors originating from poor thermal contact and temperature gradients. Thermal contact was optimized by press fitting the thermocouples 5 mm deep into the substrate from the rear end. One thermocouple was placed in the center of the substrate disk while the remaining three were placed in a uniform distribution 4 mm away from the center. The thermocouples employed were of type-K.

After the excitation of the TP, the emitted phosphorescence was collected by a plano-convex lens ($f = 300$ mm) and was focused onto the detector (PMT). The PMT was equipped with the suitable interference filter depending on the TP used. An interference filter centered on 450 nm with full-width half-maximum (FWHM) of 40 nm was employed for CdWO_4 and an interference filter centered on 656 nm (FWHM of 10 nm) for the $\text{Mg}_3\text{F}_2\text{GeO}_4\text{:Mn}$ phosphor. The PMT module used was Hamamatsu H11526-20-NF.

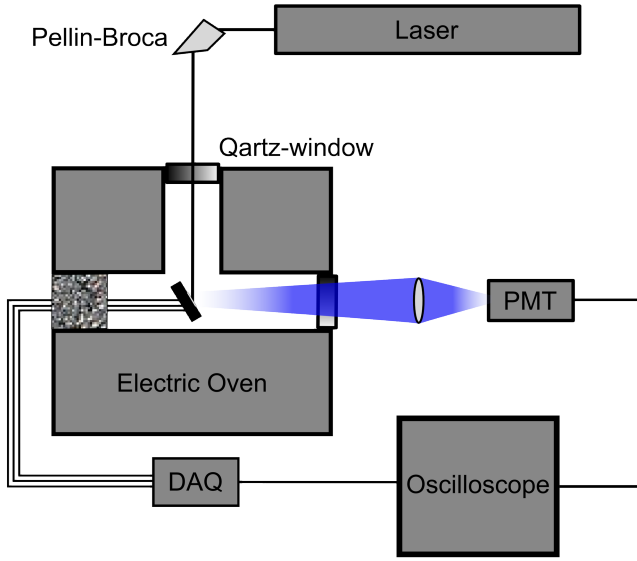


Figure 2. Schematic diagram of the developed automatic calibration's experimental setup.

During calibration, the oven is heated continuously at a constant rate. The maximum heating rate allowed is 4 K.min^{-1} . The acquisition system was composed of two components, the oscilloscope and the DAQ card. The DAQ card acquired the thermocouple temperatures and forwarded it to the oscilloscope, while the oscilloscope acquired the phosphorescence decaying signal from the PMT. The acquisition process occurring in both the DAQ and the oscilloscope was initiated simultaneously to provide the best temporal match between the temperatures and the decay curve measured. The synchronization and further processing were handled by the developed automatic routine described below. An illustration of the experimental setup is provided in fig. 2.

2.1.2 Software

The tasks of acquisition synchronizing, signal processing, hardware controlling, and data saving are all achieved using the developed automatic routine. This subsection describes the mechanism of each of the aforementioned processes. Traditionally, calibration data points are acquired when the system is at a state of thermal equilibrium. Meaning that the temperature is stable and drifts during the acquisition time are considered negligible. However, in the automated calibration, the oven is continuously heated at a slow pace, that facilitates matching the luminescence decay curve with its corresponding temperature by synchronizing the DAQ with the oscilloscope.

The next step in the automatic routine is signal processing. The signal processing phase was divided into a fast online decay time estimation algorithm and a sparsing algorithm. The online decay time estimation is first used to process the waveform and second to control the hardware settings of the following acquisition. The decay time is estimated using Ashworth's rapid decay time determination (RLD) algorithm [3-5], that is only temporarily used in the calibration routine. The RLD algorithm is characterized by its shorter computational time and comparable accuracy compared to

nonlinear least squares algorithms. Using the decay time calculated by RLD algorithm, the decay signal was terminated after five decay times (5τ) to exclude unnecessary waveform data points. After five decay times, the signal has dropped to less than one percent of the initial intensity. Then, the decay waveform was sparsed to reduce the number of data points per curve and thus reducing the saved file size. The rise-time of the phosphorescence signal is usually in the order of few nanoseconds. The sparsing algorithm was designed to maintain the native data point density of the section associated with the rise of the phosphor signal and to sparse the rest of the decaying waveform. The sparsing algorithm was designed to reduce the number of data points without influencing the quality of information represented by the waveform.

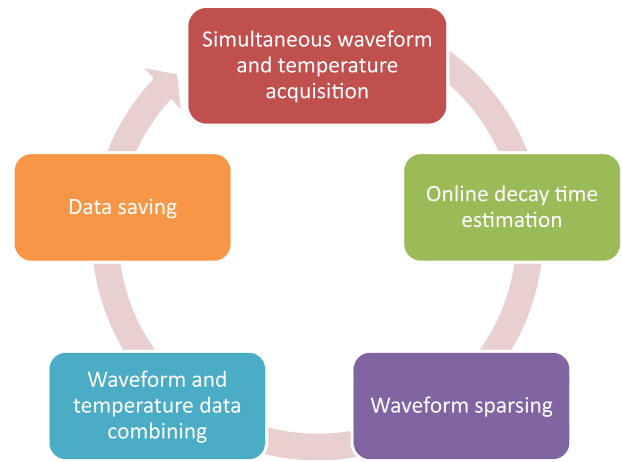


Figure 3. Illustration of the individual processes occurring in the automatic routine's processing cycle after each acquisition initiation.

The online decay time calculation is applied to each acquired waveform. This decay time is later used to adjust the oscilloscope time-base resolution to register the full decaying waveform. The vertical resolution of the oscilloscope was controlled by utilizing a moving average of the peak intensities of the waveform.

When the signal processing was completed, the processed signal was combined with its respective temperatures (from all four thermocouples). Finally, the data from the single acquisition event was saved and the system was prepared for the next acquisition. The cycle describing the processes occurring at each acquisition is represented in figure 3. It is worth mentioning that the maximum acquisition rate achieved with the current hardware was one acquisition per second.

2.2 Heat transfer study

The electric oven is heated continuously, creating thermal gradients across the substrate. Thermal gradients can produce a bias in the calibration because of the difference between temperatures experienced by the TP coating and those measured by the thermocouples. The understanding of the magnitude of thermal gradients present in the substrate is vital. For that purpose, a heat transfer model was created using COMSOL Multiphysics software to simulate the

thermal conditions of the substrate under continuous heating. The software solves the conductive heat transfer equation, presented in equation 1, using the finite element method.

$$\rho C_p \frac{\partial T}{\partial t} - \nabla \cdot (k \nabla T) = Q \quad (1)$$

Where ρ is the density (kg.m^{-3}), C_p is the specific heat capacity at constant pressure ($\text{J.kg}^{-1}.\text{K}^{-1}$), T is the absolute temperature (K), k is the thermal conductivity ($\text{W. m}^{-1}.\text{K}^{-1}$), and Q is the amount of heat (W. m^{-3}). The thermal coefficients (ρ , C_p , and k), of Hastelloy C-4, were inserted into the model from the materials library available within the COMSOL software. The heat flux, q , was set to 600 W. m^{-2} resulting in a heating rate around 4 K.min^{-1} , corresponding to the maximum heating rate allowed by the oven. The initial temperature of the model was set to 293.15 K . The model solver chosen was time dependent to observe the development of thermal gradients and temperature as function of time.

A few assumptions are needed in order for this model to be valid. The first assumption is; only conductive heating was considered significant, whereas the net heat loss due to radiative and convective processes is considered negligible. The second assumption is; all of the substrate surfaces were subjected to uniform heating from the oven. The system was thermally insulated by introducing quartz cylinders at two of the oven ports and superwool thermal insulator on the third. This made heat convection to the surrounding negligible. In addition, the substrate was suspended in the center of the furnace tube providing a uniform heating. The validity of these assumptions was confirmed by a separate model that took the whole oven geometry into account not just the substrate geometry. However, the oven model mesh size was adequate to ensure the reliability of the assumptions, but lacked the mesh resolution for detailed temperature study. Increasing the mesh density can penalty the computational time required by the COMSOL software, thus a separate model was built to solve the heat transfer equation within the substrate.

The COMSOL software divided the model geometry into smaller volumes. The heat equation was then solved for each of these small volumes. The division of the model geometry into these smaller volumes was achieved by applying a software-generated mesh. The mesh is of tetrahedral geometry. The model used a very fine mesh size ranging over a mesh element size from 0.58 down to 0.06 mm . The total number of mesh elements was around 691×10^3 elements.

3 Results and discussion

3.1 Heat transfer study

After solving the heat equation using the initial parameters, a temperature distribution across the modeled substrate volume was obtained. A three dimensional distribution of temperatures attained at time $t = 3600$ seconds is displayed in Fig. 4. The temperature spread is around 0.4 K indicating small temperature gradients across the sample. Three probing points were inserted in the model at the surface of the

substrate, at 1 mm beneath the surface and at the center (3 mm depth).

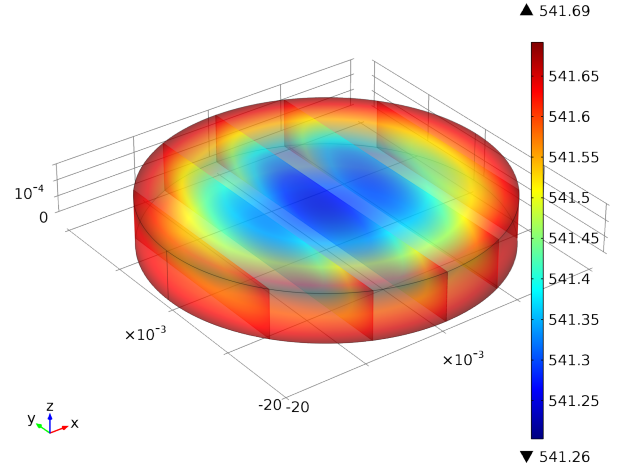


Figure 4. Three dimensional temperature distribution (K) of the Hastelloy substrate disk at $t = 3600 \text{ s}$.

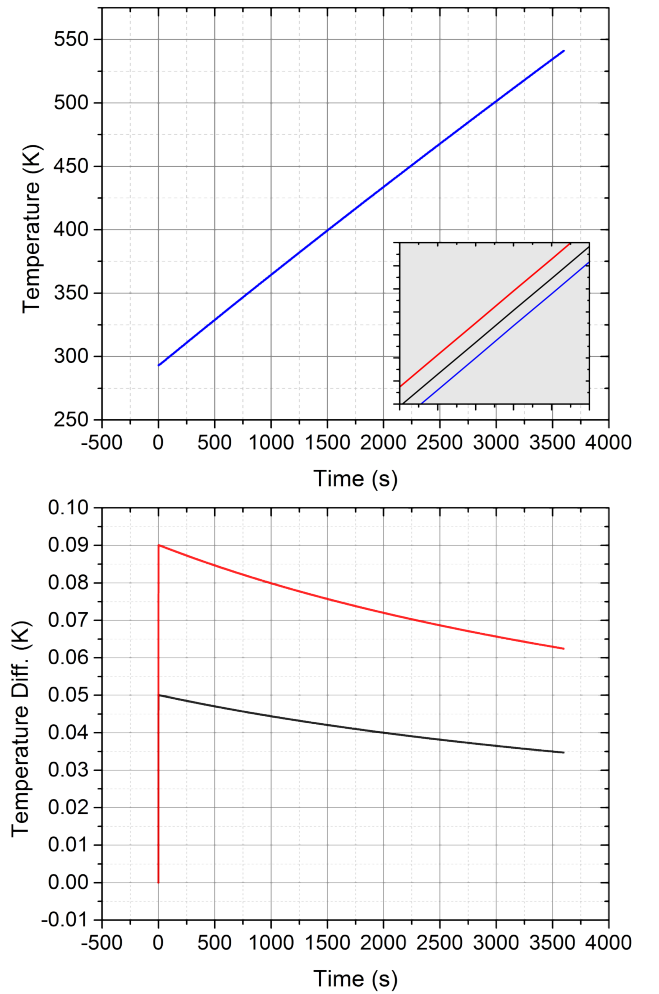


Figure 5. (Top) Temperature history at the radial center of the substrate at 0 mm depth (red), 1 mm depth (black), and 3 mm depth (blue). The inset shows a zoom of the temperature history. (Bottom) represents the difference in temperatures at the surface and at 1 mm depth (black) and at the surface and at 3 mm depth (red).

All of these probing points are located in the centre of the radial position. These points are considered enough to roughly understand the heat gradients as function of thickness, due to the symmetry of the disk and the uniformity of the heat applied upon the surfaces. The temperature history and difference for each of these points are illustrated in Fig. 5.

Starting from an initial temperature of 293.15 K and after applying the heat flux for one hour, the modelled temperatures reached a maximum value around 541.5 K. The temperature gradients across the substrate as function of depth are small. The temperature range selected for modelling is considered adequate to characterize the thermal properties of the substrate because at higher temperatures, while maintaining the same heating rate, the thermal gradients will only decrease (Fig. 5).

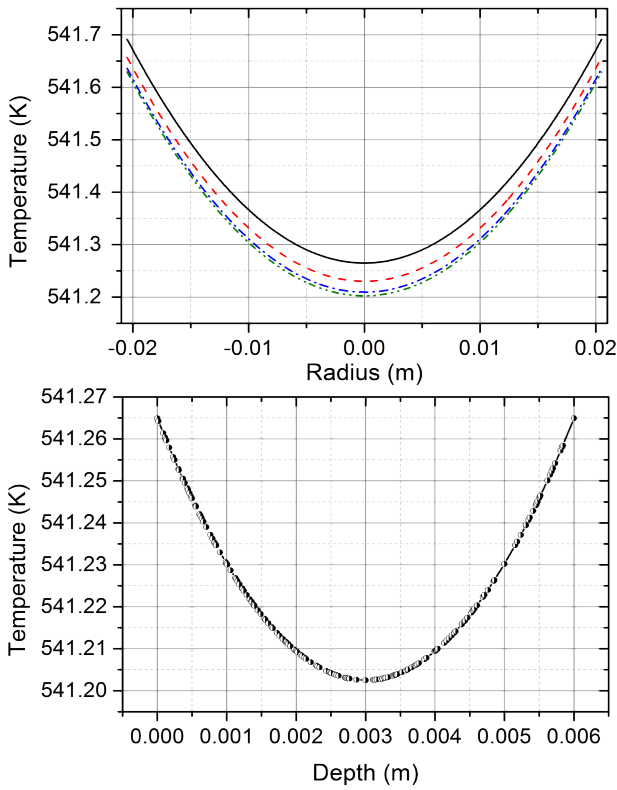


Figure 6. (Top) temperature profile at $t = 3600$ s as function of substrate disk radius, at the surface (solid black line), 1 mm depth (dashed red line), 2 mm depth (dash-dotted blue line), and at 3 mm depth (double dotted-dashed green line). (Bottom) temperature profile at $t = 3600$ s as function of depth.

To complement the data presented above and to provide a better description of the temperature profile as function depth and radial position, Figure 6 is provided. The temperature profiles have a characteristic parabolic profile due to the symmetry of the disk with respect to the z-axis and to the centre of the disk. It is worth mentioning that in a calibration, the phosphor is coated as a small disk of a diameter around 10 mm placed at the centre of the substrate disk.

This heat transfer study confirms that the thermal gradients are of negligible magnitudes up to heating rates of $4 \text{ K} \cdot \text{min}^{-1}$. Thus, the two major sources of calibration systematic error

are the thermocouples and the decay time fitting routine. The systematic error of thermocouples is of intrinsic nature and it is at its lowest in tolerance class 1 thermocouples. The installed thermocouples are of the tolerance class 1 with an inherent accuracy of either $\pm 1.5 \text{ K}$ or $\pm 0,004 \cdot |t| \text{ (K)}$ depending on the temperatures measured.

A detailed study of the relation between the evaluated phosphor temperature and thermocouple temperature in the developed automatic calibration system is presented by the authors in a complementary study [7]. The experimental study concluded that there was no temporal lag between thermocouple and phosphor temperatures even for heating rates up to $10 \text{ K} \cdot \text{min}^{-1}$.

3.2 Library-based Calibration

A conventional calibration and an automatic calibration curves for the thermographic phosphor $\text{Mg}_3\text{F}_2\text{GeO}_4\text{:Mn}$ were achieved (Fig. 7). Both calibration curves overlap well, that is an indication of the stability of the new calibration routine.

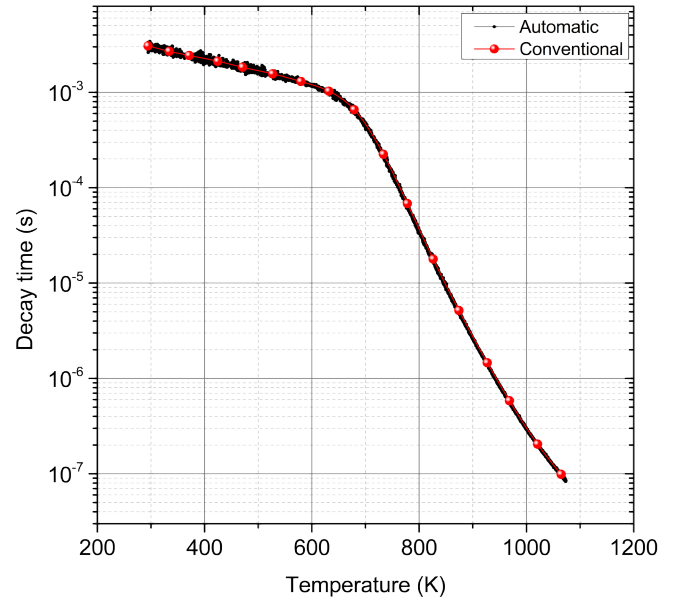


Figure 7: Automatic and conventional calibration curves for the thermographic phosphor $\text{Mg}_3\text{F}_2\text{GeO}_4\text{:Mn}$.

Two calibration curves were generated for each of the used phosphors (Fig. 8). The displayed calibration curves are composed of single acquisitions and no averaging was introduced to the curves.

The library-based calibration obtained from the automated system described earlier, allowed for the development of signal shape recognition (SSR) algorithm for TP temperature extraction [8]. This algorithm excludes the need of extracting a decay time out of the decaying waveform using fitting algorithms, and thus temperature evaluation based on decay time. The SSR algorithm calculates the temperature by matching the acquired waveform with the readily available calibration library. The best matching is reached by minimizing sum of the squared residuals. The algorithm demonstrated an improvement in accuracy of the calculated

temperature and in computational time. The SSR algorithm provides a good alternative to nonlinear least squares fitting algorithms conventionally used for decay time extraction. The SSR algorithm exhibits a high tolerance for bias in temperature calculation occurring for waveforms of low signal-to-noise ratio. In addition, the SSR algorithm performs well when using TPs that exhibit multi-exponential decays. For the SSR algorithm to work optimally a dense calibration library is necessary.

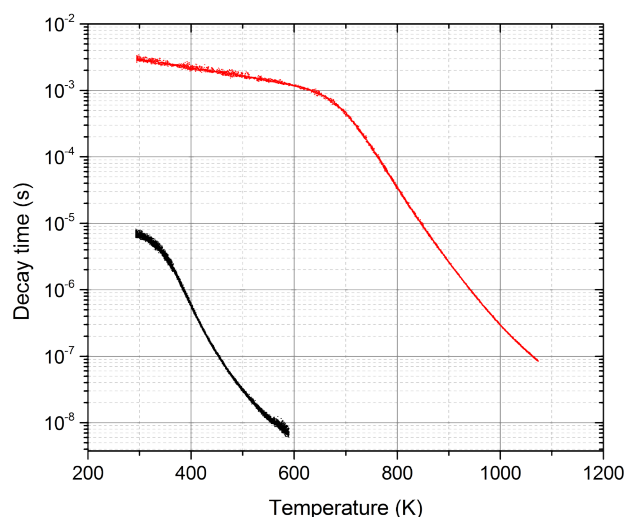


Figure 8. Library-based automated calibration of CdWO_4 (black) and $\text{Mg}_3\text{F}_2\text{GeO}_4\text{:Mn}$ (red) thermographic phosphors.

4 Conclusions

This study presented an automated system for the calibration of thermographic phosphors. The development process included software and hardware aspects. A new substrate was designed and its thermal properties were analyzed using a heat transfer model. The model provided a clear understanding of the thermal gradients occurring within the substrate. Thermal gradients at the maximum heating rate allowed were found to be negligible with a maximum spatial gradient of 0.4 K. On the software aspect, an original routine handled the synchronization, processing, and storage of the calibration data. The routine employed an online decay time estimating algorithm that provided necessary information for the adjustment of the system to the temperature dependent transient properties of the thermographic phosphors luminescence.

The finalized calibration system provided a dense calibration library, which was further exploited to develop a novel algorithm for thermographic phosphors temperature evaluation. The signal shape recognition algorithm has been shown to provide a potential alternative to conventional fitting algorithms.

The benefits of the automated calibration system are first improvement in temperature accuracy. Second, calibration duration is shortened by a factor of four due to continuous heating. Third, in spite of the reduced acquisition time a

significantly more dense calibration library is created. The latter is required for application of the SSR algorithm.

Acknowledgements

The research leading to these results has received funding from the European Union Seventh Framework Programme (FP7/2007-2011) under grant agreement no. 265861 (Helios) and from the Swedish Energy Agency within D60-2L project under grant agreement no. 30905-2.

References

- [1] P.R.N. Childs, J.R. Greenwood, and C.A. Long, *Review of temperature measurement*. Review of Scientific Instruments, 2000. **71**(8): p. 2959-2978.
- [2] A. Khalid and K. Kontis, *Thermographic Phosphors for High Temperature Measurements: Principles, Current State of the Art and Recent Applications*. Sensors, 2008. **8**(9): p. 5673-5744.
- [3] R.J. Woods, S. Scypinski, and L.J.C. Love, *Transient digitizer for the determination of microsecond luminescence lifetimes*. Analytical Chemistry, 1984. **56**(8): p. 1395-1400.
- [4] R.M. Ballew and J.N. Demas, *An error analysis of the rapid lifetime determination method for the evaluation of single exponential decays*. Analytical Chemistry, 1989. **61**(1): p. 30-33.
- [5] R.M. Ballew and J.N. Demas, *Error analysis of the rapid lifetime determination method for single exponential decays with a non-zero baseline*. Analytica Chimica Acta, 1991. **245**(0): p. 121-127.
- [6] *HASTELLOY C-4 Alloy*, I. Haynes International, Editor 2004.
- [7] F. Abou Nada, C. Knappe, X. Xu, M. Richter, and M. Aldén, *Development of an automatic routine for calibration of thermographic phosphors*. Measurement Science and Technology, 2014. **25**(2): p. 025201.
- [8] C. Knappe, K. Pfeiffer, M. Richter, and M. Aldén, *A library-based algorithm for evaluation of luminescent decay curves by shape recognition in time domain phosphor thermometry*. Journal of Thermal Analysis and Calorimetry, 2014. **115**(1): p. 545-554.